

Trace-Level, Multi-Gas Detection for Food Quality Assessment Based on Decorated Silicon Transistor Arrays

Zhen Yuan, Mallika Bariya, Hossain M. Fahad, Jingbo Wu, Rui Han, Niharika Gupta, and Ali Javey*

Multiplexed gas detection at room temperature is critical for practical applications, such as for tracking the complex chemical environments associated with food decomposition and spoilage. An integrated array of multiple silicon-based, chemical-sensitive field effect transistors (CSFETs) is presented to realize selective, sensitive, and simultaneous measurement of gases typically associated with food spoilage. CSFETs decorated with sensing materials based on ruthenium, silver, and silicon oxide are used to obtain stable room-temperature responses to ammonia (NH₃), hydrogen sulfide (H₂S), and humidity, respectively. For example, one multi-CSFET sensor signal changes from its baseline by 13.34 in response to 1 ppm of NH₃, 724.45 under 1 ppm H₂S, and 23.46 under 80% relative humidity, with sensitive detection down to 10 ppb of NH₃ and H₂S. To demonstrate this sensor for practical applications, the CSFET sensor array is combined with a custom-printed circuit board into a compact, fully integrated, and portable system to conduct real-time monitoring of gases generated by decomposing food. By using existing silicon-based manufacturing methodologies, this room-temperature gas sensing array can be fabricated reproducibly and at low cost, making it an attractive platform for ambient gas measurement needed in food safety applications.

Trace-level gas detection is crucial for safety and quality monitoring in various industrial processes such as manufacturing, agriculture, warehousing, etc.^[1,2] Advanced gas sensors are needed with robust sensing performance, minimal power consumption, miniaturized size, and scalable production. Sensors based on various operating principles have been investigated for trace-level gas detection in the past decades, including resistance-based,^[3,4] capacitance-based,^[5,6] electrochemical-based,^[7,8]

and mass-sensitive sensors,^[9] but few of these have been demonstrated to be cost, power, and size effective. For instance, the widely commercialized resistance-based metal oxide sensors must typically be operated at high temperatures to enable the adsorption interactions required for transduction.^[8,10–12] This results in higher power consumption as operation temperatures must be adjusted by a built-in heater. While other efforts have focused on the optimization of sensing materials^[4,13,14] and sensor structure,^[15] the resulting devices remain far from being practically applicable due to their limited detection sensitivity and poor reproducibility under mass fabrication.^[16] Therefore, effective gas sensing systems with minimal baseline drift, good selectivity, low hysteresis, and the ability to simultaneously measure multiple gases still need to be developed. In this context, silicon transistor-based sensors have shown significant promise, with key advantages in overcoming size limitations, low power sensing, and high sensitivity,^[17–21] making them useful for trace-level gas sensing applications required in food freshness monitoring.

Ammonia (NH₃) and hydrogen sulfide (H₂S) are two types of marker gases for spoiling food. For high-protein foods such as eggs, dairy, and meat, off-gassed NH₃ and H₂S serve as quality indicators of freshness.^[22–25] These gases can also be emitted from rotting vegetables such as corn and spinach.^[26] For simplicity, eggs and pork samples are selected for monitoring food spoilage in this work. Based on reported data, 10 mL of egg whites produces ≈100 μg of H₂S over multiple hours.^[23] After accounting for food storage volume and temperature, this means that the sensor system must be able to identify H₂S and NH₃ gases with lower than 100 ppb detection limits and negligible cross-sensitivity. While electrochemical, colorimetric, and other sensing schemes in previous work have shown promise for gas and adulteration detection, it still remains to detect gas signatures continually and at low concentration levels for monitoring spoiling food.^[24–29] Multiplexed sensing is also important—for example, humidity is another important parameter that affects food storage and spoilage,^[22,30–34] and thus should be simultaneously monitored with H₂S and NH₃. All of these requirements necessitate the deployment of sensors with high selectivity and low detection limits.

Z. Yuan, M. Bariya, Dr. H. M. Fahad, J. Wu, R. Han, N. Gupta, Prof. A. Javey
Department of Electrical Engineering and Computer Sciences
University of California, Berkeley
Berkeley, CA 94720, USA
E-mail: ajavey@berkeley.edu

Z. Yuan, M. Bariya, Dr. H. M. Fahad, J. Wu, R. Han, N. Gupta, Prof. A. Javey
Berkeley Sensor and Actuator Center
University of California, Berkeley
Berkeley, CA 94720, USA

Z. Yuan, M. Bariya, Dr. H. M. Fahad, J. Wu, R. Han, N. Gupta, Prof. A. Javey
Materials Sciences Division
Lawrence Berkeley National Laboratory
Berkeley, CA 94720, USA

 The ORCID identification number(s) for the author(s) of this article can be found under <https://doi.org/10.1002/adma.201908385>.

DOI: 10.1002/adma.201908385

In this work, n-doped bulk silicon-based chemical-sensitive field effect transistors (CSFETs) are developed for multiplexed, trace-level gas sensing in NH_3 , H_2S , and H_2O for food safety and quality monitoring. Electrically floating, thin film Ru, Ag, and SiO_x constitute as chemical gates of CSFETs to impart sensitivity towards NH_3 , H_2S , and H_2O , respectively. Compared with similar sensor topologies reported in literature, these CSFETs demonstrate stable sensing performances with superior sensitivity and ultra-low detection limits, as well as minimal hysteresis, excellent selectivity, and negligible cross-sensitivity (Table S1, Supporting Information).

The developed multi-CSFET array is integrated with a custom-designed printed circuit board (PCB) to build a portable and autonomous CSFET sensor system for multiplexed, trace-level gas detection. This device is envisioned for integration into smart fridges, providing food quality insights that could allow producers and consumers to both identify unsafe items and reduce food waste. In this work, the system is demonstrated for continuous, real-time monitoring of egg and pork belly spoilage at different storage temperatures. Significant sensor signal changes, especially towards H_2S , were detected before and during the spoilage process of the specific food items. Furthermore, the onset of food spoilage was seen to decrease with increasing temperature as expected, confirming the reliability of this system for food quality assessment. Based on the results presented here, this work paves the way towards trace-level multi-gas detection for ubiquitous food quality monitoring.

The bare CSFET was fabricated via standard silicon complementary metal oxide semiconductor (CMOS) processing as

shown in Figure S1, Supporting Information, based on our previous work.^[21] In order to keep CSFETs “on” after decoration with functional materials, their channels were lightly n-doped at the to reduce the initial threshold voltage (V_{th}) of the underlying transistors. Following lithography-based patterning of sensing materials, the complete structure of the fabricated multi-CSFET arrays is shown in Figure 1. As seen in step-by step zoom-in images from wafer-scale to device-scale (Figure 1a–d), three different types of sensors are patterned along a line to form a sensor array covering $400\ \mu\text{m} \times 450\ \mu\text{m}$. Figure 1e,f depicts the 3D schematic of the multi-CSFET array and the cross-sectional schematic of a single CSFET, respectively.

Individual CSFET units of the multi-CSFET array were decorated with different functional sensing materials to be selective towards different target gases. Due to the specific interactions of Ru-N^[35,36] and Ag-S,^[37] Ru and Ag are selected as the sensing materials for the detection of NH_3 and H_2S . Ru has been shown to catalyze NH_3 synthesis while silver nanoparticles have been shown to bind strongly to sulfur-containing compounds, making these metals attractive choices for selective gas adsorption. SiO_x was selected as the humidity-sensitive sensing material because of its abundant oxygen vacancies formed via rapid deposition.^[38] These three materials were successively decorated on the gate of the different CSFET units to functionalize the complete multi-CSFET array (Figure 1d).

To assess its potential for practical food-safety application, the multi-CSFET sensor array was tested with various levels of NH_3 , H_2S , and humidity to characterize target and cross-sensitivities of each sensor in the array as depicted in Figure 2.

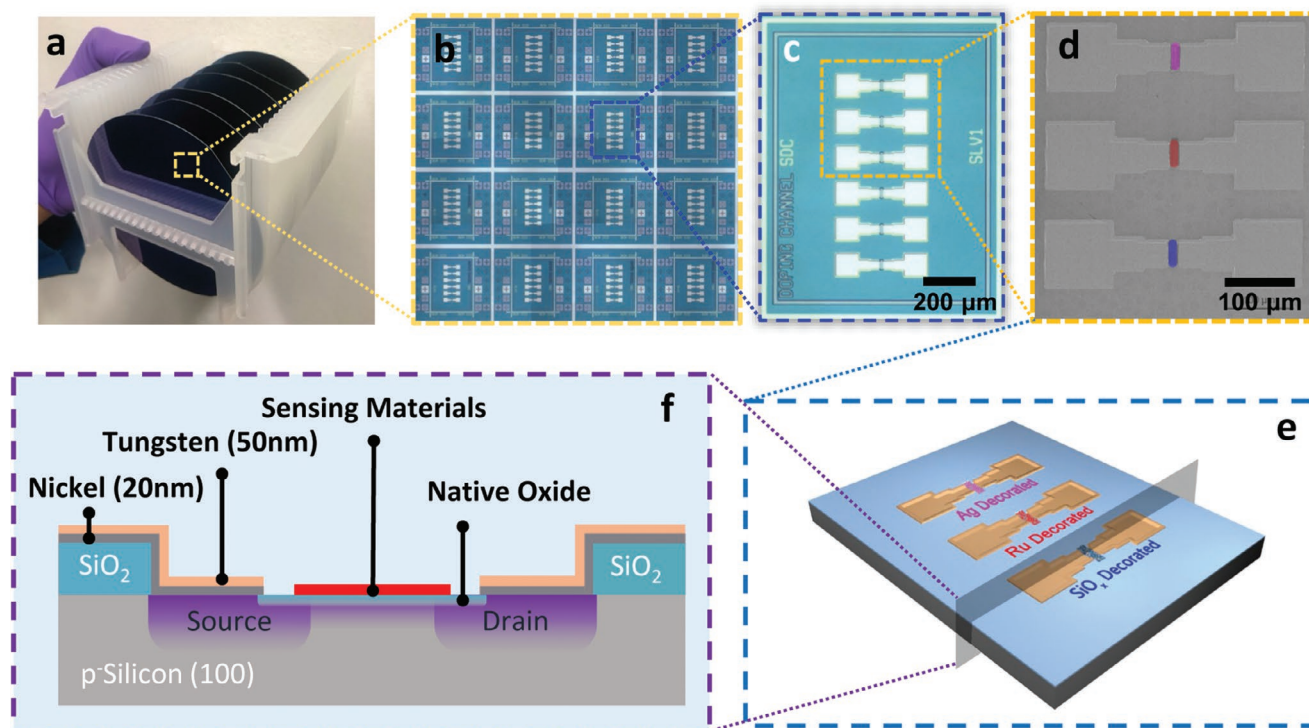


Figure 1. Device structure of CSFETs. a) Photograph of 4 in. wafers hosting CSFET arrays and b) a zoomed-in image of multiple arrays on a single wafer. c) Optical microscope image of a multimaterial-decorated CSFET array and d) corresponding scanning electron microscope (SEM) image with the position of different sensing materials marked in false color. e) 3D diagram of the multi-CSFET array and f) cross-sectional diagram of the device structure.

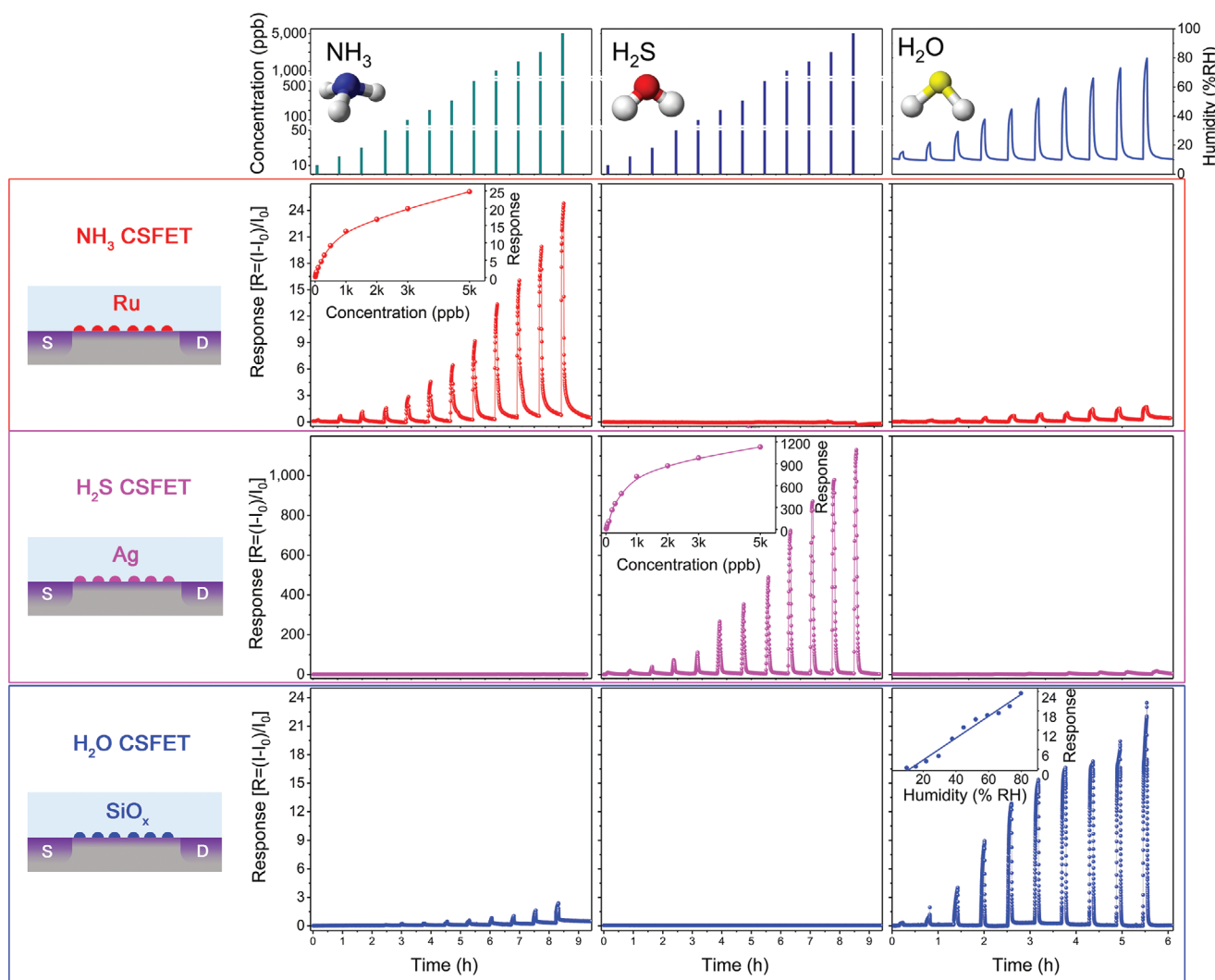


Figure 2. Sensing performance of multi-material decorated CSFETs. Response of each CSFET towards different gases with varying concentration (at $V_{DS} = 1$ V, $V_{sub} = 0$ V). Each row in the same color shows the response curves of the CSFET indicated at left (NH_3 , H_2S , and H_2O CSFET from top to bottom). Each column shows the response curves towards varying concentrations of the gas indicated at the top (NH_3 , H_2S , and humidity from left to right).

The sensor response (R) was calculated as $R = (I - I_0)/I_0$ where I and I_0 is the CSFET-measured drain current in the target gas and pure carrier gas, respectively. The limit of detection for NH_3 and H_2S was found to be as low as 10 ppb. Further, the individual sensors in the CSFET array exhibited strong preferential sensitivity towards their target gas compared to the other gases (Figure 2). Specifically, the response of the Ru-decorated CSFET towards NH_3 (13.34 at 1 ppm) was one to two order of magnitude higher than its response towards H_2S (0.05 at 1 ppm) and humidity (1.73 at 80% relative humidity (RH)). Similarly, the response of the Ag-decorated CSFET (724.45 at 1 ppm for H_2S , 0.47 at 1 ppm for NH_3 , 18.40 at 80% RH for H_2O) and the SiO_x -decorated CSFET (23.46 at 80% RH for H_2O , 0.83 at 1 ppm for NH_3 , 0.03 at 1 ppm for H_2S) showed high selectivity towards their respective target gases. The response fitting curves and parameters are listed in Figure S2, Supporting Information. The nonlinear sensor response curves of the NH_3 and H_2S CSFETs can be ascribed to the nonlinear Langmuir

relation between adsorption coverage and gas concentration as discussed in Figures S2a,b and S3, Supporting Information, as well as to inherent nonlinear transfer characteristics of FETs.^[21] Both behaviors influence the work function variation that ultimately produces the CSFET signal. Note that the NH_3 sensor's slight sensitivity to humidity stems from residual hydrophilicity of the channel surface even after the fluorosilanization treatment discussed in the Experimental Section. Measured response of other devices from the same wafer and from different batches of fabricated CSFETs is depicted in Figure S4, Supporting Information, to demonstrate reproducibility and the inherent device-to-device variability. Device-to-device performance within a batch of sensors fabricated on the same base wafer is low, giving reproducible sensor performance. However, batch-to-batch variation is expected as fabrication processes difficult to finely control in academic settings produce variation in sensing layer thickness and channel doping levels. However, this is not a fundamental limitation and the sensing layers

are found to consistently respond to their target gases across batches. Compared with recently published works, both NH_3 and H_2S CSFETs exhibit outstanding sensing performance with superior sensitivity (at least an order of magnitude higher in response per ppm), selectivity, and very low limits of detection (Table S1, Supporting Information).

Stability and hysteresis of gas sensors are critical considerations for ensuring that measured responses accurately reflect actual concentrations and to eliminate the need for repeated calibration, an important practical consideration for real-world applications. To that end, as indicated in Figure 3a, all CSFET sensors demonstrate good stability in all tested concentrations. For example, standard deviations in the responses of NH_3 , H_2S , and H_2O CSFETs towards 100 ppb pulses of NH_3 , H_2S , and 80% RH are 5.2%, 1.5%, and 1.6%, respectively. The slight increase in peak signal response is actually identical to the slight drift in baseline signal between cycles. Allowing more time for sensor recovery between cycles can remove this baseline change. The average response of the NH_3 CSFET towards 10 ppb of NH_3 is 0.20 with standard deviation of 0.016. The lowest tested concentration of NH_3 that is resolved by the NH_3 CSFETs is 10 ppb. Similarly, the H_2S CSFET can detect down to a tested concentration of 10 ppb H_2S . Figure S5, Supporting Information, shows sensor stability over a longer duration, comparing sensor

responses after fabrication with those after storage for a month at ambient conditions. Sensor performance is retained after a month and expected to last even longer due to the CSFET's robust inorganic sensing layers. Multi-year experimental stability tests are ongoing. Figure 3b shows that the response variations between increasing and decreasing concentration of 100 ppb of NH_3 , H_2S , and 55% RH are 15.8%, 1.7%, and 1.2%, respectively, indicating low hysteresis. Additionally, the selectivity of the multi-CSFET array against several common air pollutants, namely, CO , SO_2 , NO_2 , and CH_2O , was tested due to their possible existence in ambient and practical sensing environments. NH_3 and H_2S are two of the most prominent gases emitted in spoiling meat and poultry,^[22–25] typically eclipsing other emitted components, so low interference from air pollutants is a key marker of selectivity. As indicated by the response bars and overlaying values in Figure 3c, the CSFET sensors show negligible response to these common atmospheric pollutants.

In summary, the presented multi-CSFET array demonstrates stable performance with superior sensitivity towards trace-level target gases and negligible cross-sensitivity, showcasing its strong potential application in food spoilage and waste monitoring.

Since NH_3 , H_2S , and humidity are the main constituent gases released from high-protein foods, monitoring their

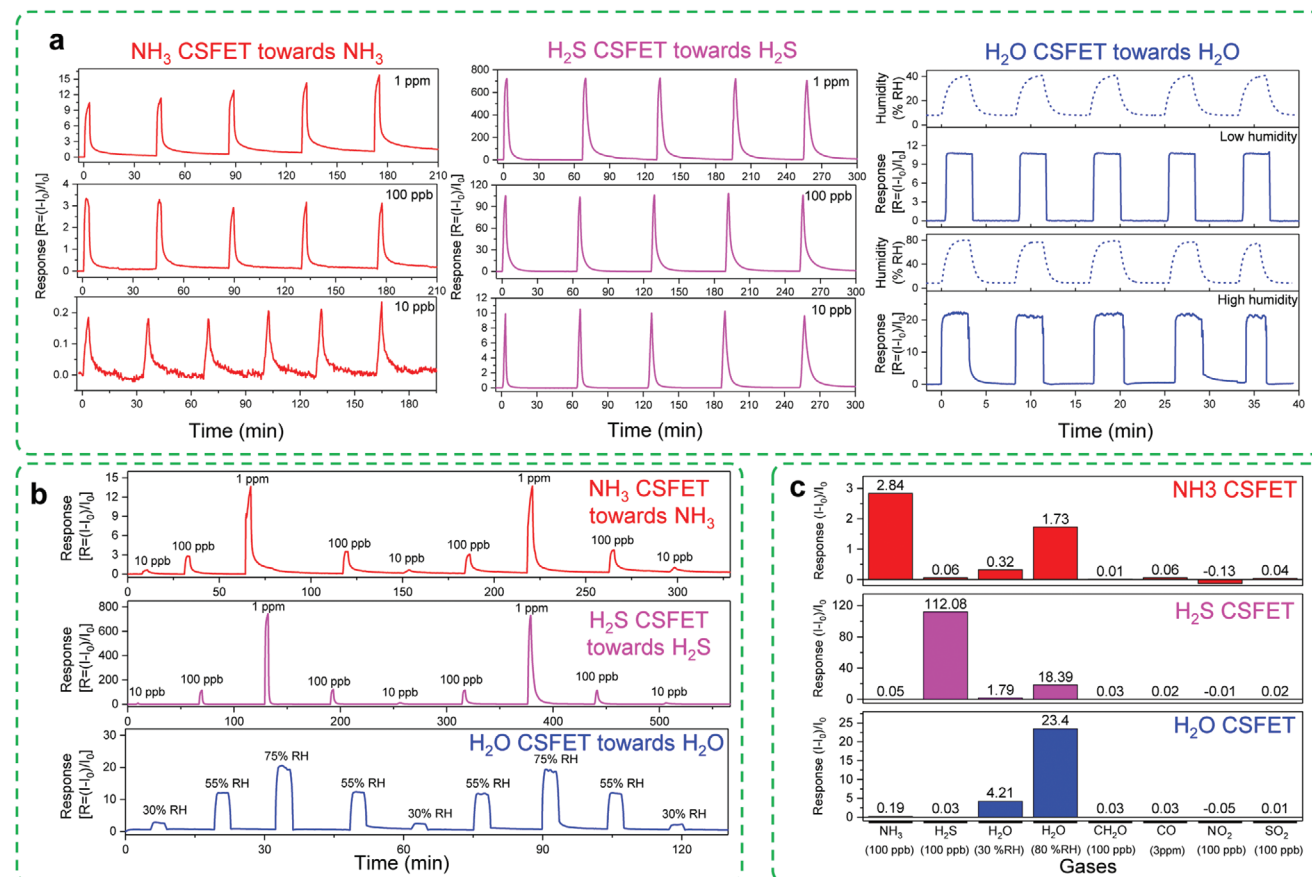


Figure 3. Repeatability and hysteresis of CSFETs. a) Responses of the NH_3 CSFET, H_2S CSFET, and H_2O CSFET to identical pulses of different target gas concentrations show repeatable performance. b) CSFET responses to cycled target gas concentrations are largely unaffected by whether the concentration is increased or decreased to a particular level, indicating low hysteresis. c) Selectivity testing of the CSFETs reveals they respond more strongly to their target gas ($V_{\text{DS}} = 1 \text{ V}$, $V_{\text{sub}} = 0 \text{ V}$).

evolution during the spoilage process can be used as a freshness indicator of such food items.^[22,23] To that end, the presented multi-CSFET array (Figure S6, Supporting Information) is a compact, autonomous system for real-time gas detection and data read-out, making it an excellent food spoilage monitoring technology.

The food spoilage tests are performed at different temperatures to verify the relationship between food spoilage time and storage temperature. We empirically expect the onset of food spoilage to occur earlier at higher temperatures, and by comparing the gas sensor results to this expectation, we seek to verify the performance of the CSFET system. Temperature-based tests of spoilage time, therefore, demonstrate platform function. Pork belly and eggs were chosen as representative foods for monitoring freshness and spoilage. The food sample and multi-CSFET array were put at opposite ends of the storage chamber to minimize the influence of temperature on the gas sensor response as shown in Figure S7, Supporting Information. Relative placement of the food sample and CSFET is not critical, as fast gas diffusion within the sealed container produces low time delays between any two points where the sensor might be placed. The side with the food sample was kept at a roughly controlled temperature using an ice bag or heater to generate low (≈ 10 °C) or high (≈ 50 °C) temperatures,

respectively. Note that the CSFET platform could be used at even lower temperatures (including the 4 °C or lower temperature typically used in food refrigeration), and while sensor sensitivity may be temperature-dependent, the CSFETs' ability to interact with and respond to their target gases will not be appreciably altered. In order to accelerate the rotting process for platform demonstration purposes, a hole was artificially created in the eggshell of all the tested eggs to expose the egg white. The associated temporal gas concentration curves are shown in Figure 4a–c. To assist comparison, all sensor signals are converted into concentration readings based on the fitting equations shown in Figure S2, Supporting Information. As seen in Figure 4a–c, once the egg was put into the chamber, the NH_3 CSFET and H_2O CSFET immediately began responding while the H_2S CSFET response remained low, possibly due to early emission of NH_3 and H_2O that originate from bioactivity of native components or bacteria within the egg. Over time, the concentration of H_2S rose prominently, indicating the onset of food spoilage.^[22,39] The NH_3 profile does not show a corresponding sudden change as rotting eggs have a predominant sulfide signature. This rotting process continued with all signals gradually leveling off. Finally, the container was opened to release the gases and all CSFET readings went down to their original baselines, demonstrating the reversibility of this sensor

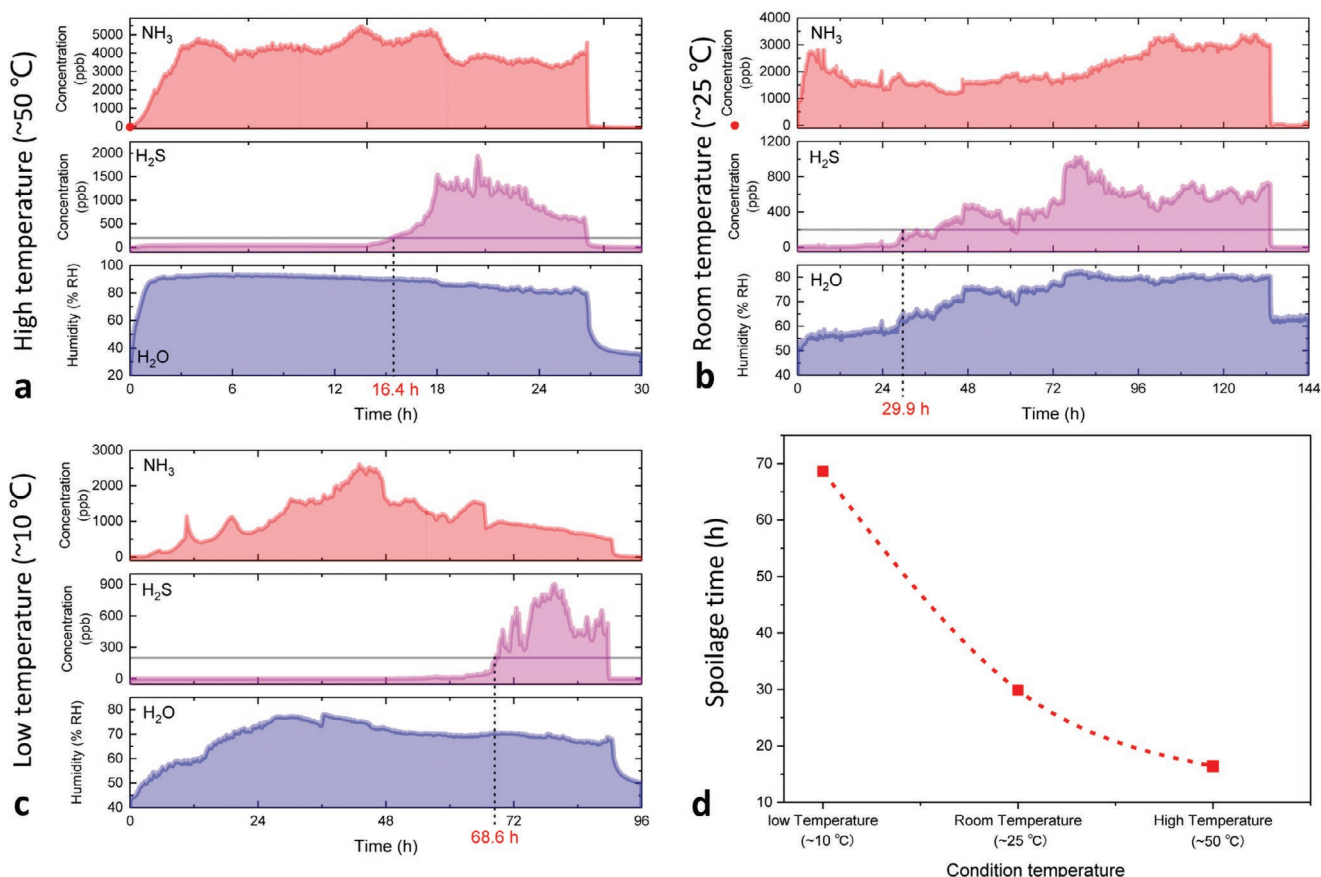


Figure 4. Egg spoilage tracking over varying food storage temperatures. Dynamic tracking of gas concentrations at different storage temperature: a) high temperature (≈ 50 °C), b) room temperature (≈ 25 °C), and c) low temperature (≈ 10 °C). The estimated onset time of spoilage is determined by the rotting egg's dominant H_2S signature and is labeled with a dashed line and the time. d) The relationship between spoilage onset time and storage temperature based on test results.

system. By considering the temporal concentration curves of H_2S , the time of rapid concentration increase can be regarded as the start of the rotting process with 200 ppb as a threshold indicating spoilage. The rationale for this is as follows: because gas concentrations depend on enclosure volume and sample mass among other features, there is no clear reference for the expected gas concentration at each stage of spoilage. However, previous research indicates that for degrading protein-rich foods such as fish, ppb to low ppm levels can be expected for spoiled food.^[40] After accounting for features of our setup, we choose 200 ppb as a threshold concentration to indicate food spoilage, a cutoff that in future can be modified to account for different foods or storage conditions. As seen in Figure 4d, the time to spoilage associated with surpassing this 200 ppb threshold is 68.6, 29.9, and 16.4 h at low, room, and high temperatures, respectively. The onset of spoilage occurs later at lower temperatures as expected, likely due to decreased activity at lower temperatures of the bacteria that contribute to food degradation. While the exact functional form of the temperature-dependence curve could depend on various factors, including the composition of this particular batch of eggs and other environmental considerations, this general increase in onset time with decreasing temperatures is consistent with existing knowledge that cooler environments delay spoilage. To verify that the

gas-sensing platform consistently shows this trend, this egg spoilage trial is repeated in Figure S8, Supporting Information, with comparable results. Note that while the curves in both trials monotonically decrease with temperature, the exact functions differ due to the complex history of the particular food sample, different delivery methods or storage condition, etc. We, therefore, do not expect the concentration curves of all food spoilage trials to be identical, and more comprehensive studies will be needed in future to better interpret gas sensor results. For visual comparison, photographs of a progressively spoiling egg in a test tube are captured at different times (0, 2, and 5 days at room temperature) in Figure S9a, Supporting Information, to visually confirm that the egg does indeed rot over the timespan indicated by the gas sensor results.

To further demonstrate this system for food spoilage detection, a similar strategy is applied for the pork belly spoilage test. Pork belly is chosen as it is known to release both NH_3 and H_2S among other gases during rotting, so we expect to obtain both sulfide and NH_3 signatures during spoilage.^[41] Real-time monitoring of released gases under different temperature is shown in Figure 5a–c. Overall, a similar concentration trend is observed compared to the spoiling egg, but with an additional expected increase in NH_3 levels during decay. The concentration of H_2S and NH_3 gases is higher at higher temperatures,

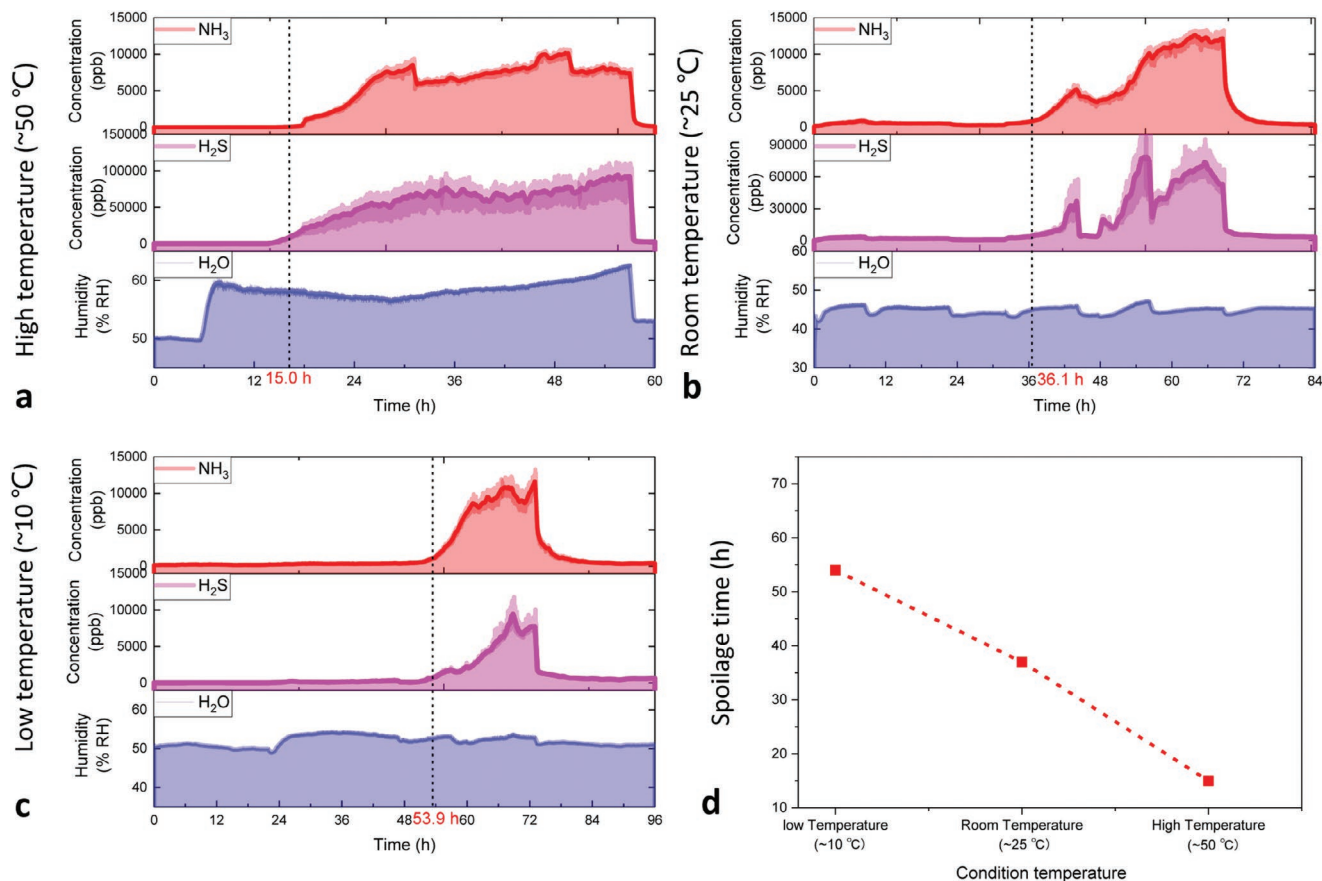


Figure 5. Pork belly spoilage tracking over varying food storage temperatures. Measurement results of sensors at different storage temperature: a) high temperature (≈ 50 °C), b) room temperature (≈ 25 °C), and c) low temperature (≈ 10 °C). The spoilage time is determined by both the NH_3 and H_2S signatures of the rotting meat, and is labeled with a dashed line and time. d) The relationship between spoilage time and storage temperature based on test results.

due to higher bacterial colony activity. When the test chamber is opened, the H₂S and NH₃ sensors exponentially recover to their original values. Over the duration of the test, the humidity sensor shows a relatively stable response. In future, more comprehensive spoilage tests will be needed to explain this and more deeply explore when and how certain gas levels elevate. To compare the onset of rotting at different temperature, 200 ppb is again chosen as the threshold concentration. The time to when both H₂S and NH₃ sensors reach 200 ppb is extracted and plotted versus temperature in Figure 5d, estimating the onset of spoiling at 54.0, 36.1, and 15.0 h at low, room, and high temperatures, respectively. The time to spoilage of the pork belly is lower with higher storage temperature, as expected. To verify this result, the pork belly spoilage trial is repeated in Figure S10, Supporting Information, with comparable results. To visually confirm spoilage, optical images of the pork belly when fresh and then after spoilage are shown in Figure S9b, Supporting Information, revealing a noticeably duller sample after spoilage. Overall, this demonstration with dynamic egg and pork belly spoilage monitoring highlights the capability of the multi-CSFET array system to quantitatively gauge food freshness. To further develop the utility of this system, more comprehensive food spoilage tests can be conducted and analyzed with statistical methods to identify spoilage thresholds and characteristic spoilage profiles for different foods.

In summary, we develop a high-performance multi-CSFET array for trace-level, multi-gas sensing and demonstrate its ability to assess complex gaseous environments for practical applications. Ru, Ag, and SiO_x were identified as sensing materials towards NH₃, H₂S, and humidity, respectively, and were independently functionalized on the gates of three CSFET units. The resulting sensors demonstrate superior sensitivity, low limit of detection, and minimal hysteresis towards their target gases with negligible cross-sensitivity and baseline drift. The multi-CSFET array was integrated with custom PCB and circuitry to conduct proof-of-concept measurements of food spoilage. Overall, the CSFET sensor arrays demonstrate high performance for trace-level gas sensing, can be manufactured reliably and at low cost with traditional silicon processing, and can be robustly integrated with compact circuitry to enable convenient and autonomous gas measurements in ambient conditions. Beyond food spoilage monitoring, this platform can be adapted to different applications by using alternate functional sensing materials, for example, to detect gaseous markers of lung or gastrointestinal disease present at ppb levels in exhaled breath, or to detect toxic gas leaks in industrial manufacturing.^[42] In closing, the presented multi-CSFET array system also has broad prospects in practical applications such as in health, safety, and air quality monitoring, due its portability and durability.

Experimental Section

CSFET Fabrication Process: CSFETs were fabricated using conventional CMOS processing. As depicted in Figure S1, Supporting Information, after standard cleaning, a (100) orientation p⁻ silicon wafer was subjected to a three-step dry (5 min)-wet (55 min)-dry (5 min) oxidation process at 1000 °C, atmospheric pressure, in order to thermally grow a ≈350 nm silicon dioxide as insulation layer. Then, the source and

drain doping regions were patterned by standard photolithography processes, followed with a wet etching process using 5:1 buffered hydrofluoric acid for 5 min. The source and drain doping was obtained by ion implantation (4.5e¹⁴ cm⁻², phosphorus, 15 keV) and activated by rapid thermal annealing (RTA) at 1050 °C for 30 s in N₂ to form the n⁺⁺ doped regions. After that, the channel region was etched and doped by the same process as source-drain but with different implantation parameter (5e¹¹ cm⁻², phosphorus, 18 keV). The channel region became n⁻ after RTA at 900 °C for 1 s in N₂. Finally, another photolithography step was utilized to form the contact region. A total of 20 nm nickel and 50 nm tungsten were sputtered successively as contacts followed with lifting-off in acetone. To obtain ohmic contact, the as-prepared wafer was annealed by RTA at 420 °C for 5 min in forming gas to form nickel silicidation (NiSi). To decorate the bare CSFET, different materials were deposited on the CSFET channel by evaporation (Ru: e-beam, 0.1 Å s⁻¹, 1 nm; Ag: thermal, 0.1 Å s⁻¹, 1 nm; SiO_x: e-beam, 2 Å s⁻¹, 3 nm). For the NH₃ and H₂S CSFETs, in order to reduce the response of native oxide to humidity, the surface of the CSFETs was treated by O₂ plasma and trichloro(1H,1H,2H,2H-perfluorooctyl)silane (Sigma-Aldrich, 97%) vapor successively before evaporation. The CSFET fluorosilanization process is as follows: the CSFET array and a slide of glass were put into a vacuum desiccator. Several drops of trichloro(1H,1H,2H,2H-perfluorooctyl)silane were dropped onto the glass. The desiccator was capped and vacuumed to accelerate the evaporation of trichloro(1H,1H,2H,2H-perfluorooctyl)silane. The CSFET array was taken out after 1–2 h. Finally, the decorated CSFETs were annealed in forming gas at 150 °C for 1 h.

Standard Sensor Measurement Apparatus: All gas-sensing experiments, including food spoilage tests, were conducted in a walk-in fume hood. CSFET array chips were bonded with a 28-pin J-bend leaded chip carrier. For standard gas tests, the current signals were acquired by a LabVIEW-controlled data acquisition unit (NI USB-6259, National Instruments). A Keithley 428 current amplifier was used to bias the CSFET. The testing gas was produced by mixing synthetic air-diluted standard gases (MESA International Technologies, Inc.) with house-compressed dry air at a calibrated concentration through mass flow controllers (Alicat Scientific, Inc.). The typical flow rate of target gases and carrier gas was 1–100 sccm and 1 slm. The humidity was generated by two mass flow controllers, one of which was connected with a bubbler and condenser to produce moisture. The humidity was monitored by a commercial humidity sensor (model SHT2x, Sensirion AG). The current characteristics for validation were measured by Keysight 4155C semiconductor parameter analyzer.

Food Spoilage Test Circuit: In the food spoilage tests, current was acquired by DAQ (NI USB-6259, National Instruments) with Keithley 428 current amplifier or a portable sensor system as follows. The egg spoilage data as shown in Figure 4b were acquired by portable device to demonstrate the properties of portable sensor system. The overall portable system worked as a differential pulse voltammetry measurement circuit comprising three major parts: power, signal conditioning, and transmission (Figure S6a, Supporting Information). Figure S6b, Supporting Information, shows an image of the portable CSFET system. The location of the CSFET array and the integrated circuit components is labeled with different colors. For the plug-and-use purpose, the universal serial bus (USB) was selected as the circuit power supply. It can support current up to 500 mA, which is more than enough for this circuit. LT1006 (Linear Technology) single-supply operation amplifier accompanied with a resistor was chosen to make the transimpedance amplifier to convert CSFET's current signal into voltage signal. In order to maintain the full measuring range of the microcontroller's analog to digital converters (ADC), a negative voltage generator based on NE555 timer (Texas Instruments, Inc.) biases the source of the CSFET in a negative voltage while the positive input of LT1006 is connected to ground. After this, the voltage signal was fed into a SAM D21 Cortex-M0+ (32 bits ARM) (Microchip Technology) microcontroller's ADC and the pre-programmed infinite impulse response low pass filter used to denoise the signal as shown in the signal conditioning diagram (Figure S6c, Supporting Information). The microcontroller can be programmed on-board by Joint Test Action Group programmer or USB after burning a bootloader into it. Microcontroller sends processed data to a PC via USB.

Supporting Information

Supporting Information is available from the Wiley Online Library or from the author.

Acknowledgements

A.J. acknowledges the Bakar Fellows Program in funding this research work. Z.Y. was financial supported by China Scholarship Council (CSC). The authors thank all the group member for their enlightening discussion and support, and particularly Mr. Wenbo Ji, Miss Hnin Y. Nyein, and Dr. Lu Li for their input during the preparation of this article.

Conflict of Interest

H.M.F. and A.J. declare competing financial interests in equity on shares of Serinus Labs, Inc. The other authors declare no conflict of interest.

Author Contributions

Z.Y. and A.J. conceived the idea for the project and designed the experiments. Z.Y. and H.M.F. fabricated the CSFET. M.B. contributed to the optimization of the CSFET. J.W. and R.H. contributed to the PCB design. Z.Y. and N.G. measured and analyzed the sensing performance. A.J. supervised the project. All authors discussed the results and revised the article.

Keywords

CSFET, food spoilage monitoring, multi-gas detection, silicon-based transistor array, trace-level sensing

Received: December 21, 2019

Revised: February 28, 2020

Published online: April 13, 2020

- [1] L. A. Mercante, V. P. Scagion, F. L. Migliorini, L. H. C. Mattoso, D. S. Correa, *TrAC, Trends Anal. Chem.* **2017**, 91, 91.
- [2] S. Gupta Chatterjee, S. Chatterjee, A. K. Ray, A. K. Chakraborty, *Sens. Actuators, B* **2015**, 221, 1170.
- [3] H. Tai, Y. Jiang, G. Xie, J. Yu, X. Chen, Z. Ying, *Sens. Actuators, B* **2008**, 129, 319.
- [4] Z. Ye, H. Tai, T. Xie, Y. Su, Z. Yuan, C. Liu, Y. Jiang, *Mater. Lett.* **2016**, 165, 127.
- [5] B. S. NoreMBERG, R. M. Silva, O. G. Paniz, J. H. Alano, M. R. F. Gonçalves, S. I. Wolke, J. Labidi, A. Valentini, N. L. V. Carreño, *Sens. Actuators, B* **2017**, 240, 459.
- [6] O. Yassine, O. Shekhah, A. H. Assen, Y. Belmabkhout, K. N. Salama, M. Eddaoudi, *Angew. Chem., Int. Ed.* **2016**, 55, 15879.
- [7] G. Jiang, M. Golezdzinowski, F. J. E. Comeau, H. Zarrin, G. Lui, J. Lenos, A. Veileux, G. Liu, J. Zhang, S. Hemmati, J. Qiao, Z. Chen, *Adv. Funct. Mater.* **2016**, 26, 1729.
- [8] C. Wang, X. Li, F. Xia, H. Zhang, J. Xiao, *Sens. Actuators, B* **2016**, 223, 658.
- [9] S. Wang, G. Xie, H. Tai, Y. Su, B. Yang, Q. Zhang, X. Du, Y. Jiang, *Nano Energy* **2018**, 51, 231.
- [10] X. Li, C. Shao, D. Lu, G. Lu, X. Li, Y. Liu, *ACS Appl. Mater. Interfaces* **2017**, 9, 44632.
- [11] S. Moon, N. M. Vuong, D. Lee, D. Kim, H. Lee, D. Kim, S.-K. Hong, S.-G. Yoon, *Sens. Actuators, B* **2016**, 222, 166.
- [12] A. S. M. Iftekhar Uddin, D.-T. Phan, G.-S. Chung, *Sens. Actuators, B* **2015**, 207, 362.
- [13] M. Donarelli, S. Prezioso, F. Perrozzi, F. Bisti, M. Nardone, L. Giancaterini, C. Cantalini, L. Ottaviano, *Sens. Actuators, B* **2015**, 207, 602.
- [14] S. Cui, H. Pu, S. A. Wells, Z. Wen, S. Mao, J. Chang, M. C. Hersam, J. Chen, *Nat. Commun.* **2015**, 6, 8632.
- [15] S. Han, X. Zhuang, W. Shi, X. Yang, L. Li, J. Yu, *Sens. Actuators, B* **2016**, 225, 10.
- [16] M. Righettoni, A. Amann, S. E. Pratsinis, *Mater. Today* **2015**, 18, 163.
- [17] T. Xie, G. Xie, H. Du, Y. Zhou, F. Xie, Y. Jiang, H. Tai, *IEEE Sens. J.* **2016**, 16, 1865.
- [18] B. R. Takulapalli, *ACS Nano* **2010**, 4, 999.
- [19] B. R. Takulapalli, G. M. Laws, P. A. Liddell, J. Andréasson, Z. Erno, D. Gust, T. J. Thornton, *J. Am. Chem. Soc.* **2008**, 130, 2226.
- [20] H. M. Fahad, H. Shiraki, M. Amani, C. Zhang, V. S. Hebbbar, W. Gao, H. Ota, M. Hettick, D. Kiriya, Y.-Z. Chen, Y.-L. Chueh, A. Javey, *Sci. Adv.* **2017**, 3, e1602557.
- [21] H. M. Fahad, N. Gupta, R. Han, S. B. Desai, A. Javey, *ACS Nano* **2018**, 12, 2948.
- [22] J. M. Jay, *J. Milk Food Technol.* **1972**, 35, 467.
- [23] A. C. Germs, *J. Sci. Food Agric.* **1973**, 24, 7.
- [24] G. Barandun, M. Soprani, S. Naficy, M. Grell, M. Kasimatis, K. L. Chiu, A. Ponzoni, F. Güder, *ACS Sens.* **2019**, 4, 1662.
- [25] N. Tang, C. Zhou, L. Xu, Y. Jiang, H. Qu, X. Duan, *ACS Sens.* **2019**, 4, 726.
- [26] O. Erkmen, T. F. Bozoglu, in *Food Microbiology: Principles into Practice* (Eds: O. Erkmen, T. F. Bozoglu), Wiley, Chichester **2016**.
- [27] H. Xiao-wei, Z. Xiao-bo, S. Ji-yong, L. Zhi-hua, Z. Jie-wen, *Trends Food Sci. Technol.* **2018**, 81, 90.
- [28] I. M. Apetrei, C. Apetrei, *Sens. Actuators, B* **2016**, 234, 371.
- [29] P. Kumar, P. K. Sarswat, M. L. Free, *Sci. Rep.* **2018**, 8, 3348.
- [30] Z. Ma, P. Chen, W. Cheng, K. Yan, L. Pan, Y. Shi, G. Yu, *Nano Lett.* **2018**, 18, 4570.
- [31] S. Matindoust, A. Farzi, M. Baghaei Nejad, M. H. Shahrokh Abadi, Z. Zou, L.-R. Zheng, *J. Mater. Sci.: Mater. Electron.* **2017**, 28, 7760.
- [32] C.-F. Chow, P.-Y. Ho, D. Sun, Y.-J. Lu, W.-L. Wong, Q. Tang, C.-B. Gong, *Food Chem.* **2017**, 216, 382.
- [33] F. Hindle, L. Kuuliala, M. Mouelhi, A. Cuisset, C. Bray, M. Vanwolleghem, F. Devlieghere, G. Mouret, R. Bocquet, *Analyst* **2018**, 143, 5536.
- [34] J.-E. Hyun, J.-H. Kim, Y.-S. Choi, E.-M. Kim, J.-C. Kim, S.-Y. Lee, *J. Food Saf.* **2018**, 38, e12433.
- [35] M. Kitano, S. Kanbara, Y. Inoue, N. Kuganathan, P. V. Sushko, T. Yokoyama, M. Hara, H. Hosono, *Nat. Commun.* **2015**, 6, 6731.
- [36] H. Abe, Y. Niwa, M. Kitano, Y. Inoue, M. Sasase, T. Nakao, T. Tada, T. Yokoyama, M. Hara, H. Hosono, *J. Phys. Chem. C* **2017**, 121, 20900.
- [37] C. Wang, Y. Ding, X. Bi, J. Luo, G. Wang, Y. Lin, *Sens. Actuators, B* **2018**, 264, 404.
- [38] A. Mehonic, A. L. Shluger, D. Gao, I. Valov, E. Miranda, D. Ielmini, A. Bricalli, E. Ambrosi, C. Li, J. J. Yang, Q. Xia, A. J. Kenyon, *Adv. Mater.* **2018**, 30, 1801187.
- [39] L. Gram, P. Dalgaard, *Curr. Opin. Biotechnol.* **2002**, 13, 262.
- [40] P. M. Schweizer-Berberich, S. Vaihinger, W. Göpel, *Sens. Actuators, B* **1994**, 18, 282.
- [41] L. Huang, J. Zhao, Q. Chen, Y. Zhang, *Food Chem.* **2014**, 145, 228.
- [42] K. H. Kim, S. A. Jahan, E. Kabir, *TrAC, Trends Anal. Chem.* **2012**, 33, 1.